Volume 25
Number 2
14 January 2023
Pages 881–1374

PCCP

Physical Chemistry Chemical Physics

rsc.li/pccp

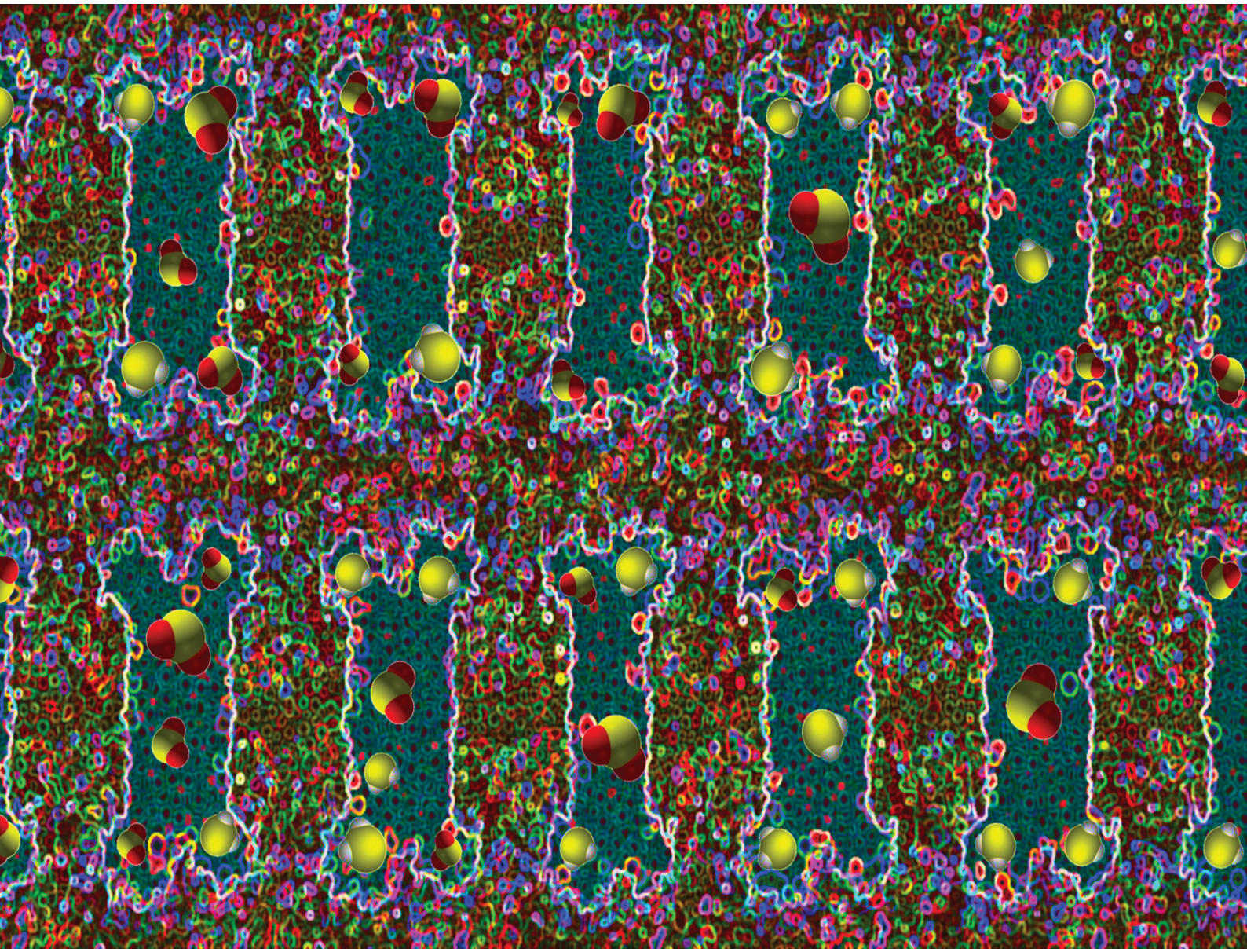

ISSN 1463-9076

ROYAL SOCIETY OF CHEMISTRY

PAPER

S. Grubišić, M. Hochlaf *et al.*
Selective adsorption of sulphur dioxide and hydrogen sulphide by metal–organic frameworks

PCCP

PAPER

View Article Online
View Journal | View Issue

Cite this: *Phys. Chem. Chem. Phys.*, 2023, **25**, 954

Selective adsorption of sulphur dioxide and hydrogen sulphide by metal–organic frameworks†

S. Grubišić, *[a] R. Dahmani, ‡[bc] I. Djordjević, [a] M. Sentić [a] and M. Hochlaf *[b]

The removal of highly toxic gasses such as SO_2 and H_2S is important in various industrial and environmental applications. Metal organic frameworks (MOFs) are promising candidates for the capture of toxic gases owing to their favorable properties such as high selectivity, moisture stability, thermostability, acid gas resistance, high sorption capacity, and low-cost regenerability. In this study, we perform first principles density functional theory (DFT) and grand-canonical Monte Carlo (GCMC) simulations to investigate the capture of highly toxic gases, SO_2 and H_2S, by the recently designed ZTF and MAF-66 MOFs. Our results indicate that ZTF and MAF-66 show good adsorption performances for SO_2 and H_2S capture. The nature of the interactions between H_2S or SO_2 and the pore surface cavities was examined at the microscopic level. SO_2 is adsorbed on the pore surface through two types of hydrogen bonds, either between O of SO_2 with the closest H of the triazole 5-membred ring or between O of SO_2 with the hydrogen of the amino group. For H_2S inside the pores, the principal interactions between H_2S and surface pores are due to a relatively strong hydrogen bonds established between the nitrogens of the organic part of MOFs and H_2S. Also, we found that these interactions depend on the orientation of SO_2/H_2S inside the pores. Moreover, we have studied the influence of the presence of water and CO_2 on H_2S and SO_2 capture by the ZTF MOF. The present GCMC simulations reveal that the addition of H_2O molecules at low pressure leads to an enhancement of the H_2S adsorption, in agreement with experimental findings. However, the presence of water molecules decreases the adsorption of SO_2 irrespective of the pressure used. Besides, SO_2 adsorption is increased in the presence of a small number of CO_2 molecules, whereas the presence of carbon dioxide in ZTF pores has an unfavorable effect on the capture of H_2S.

Received 15th September 2022,
Accepted 22nd November 2022

DOI: 10.1039/d2cp04295a

rsc.li/pccp

I. Introduction

Sulphur is an essential element of living systems, and the sulphur cycle plays a prominent role in environmental and climate changes. Sulphur bearing acid gases such as hydrogen sulphide (H_2S) and sulphur dioxide (SO_2) are naturally released into the environment through volcanic eruptions, hot springs, gas streams, breakdown of organic matter, and anaerobic bacterial reduction.[1,2] The anthropogenic sources significantly increase their atmospheric concentrations,[1,2] which have a major impact on the natural sulphur cycle.[3,4] Both gases are highly toxic to humans and the environment. Indeed, they have a detrimental effect on human and animal health and represent precursors for acid rains, causing an increase in soil acidity and the availability of heavy metals.[5,6] Also, recent studies revealed that high concentrations of SO_2 and NO_x strongly contribute to the $PM_{2,5}$ particle formation.[7] In fact, CO, CO_2, O_3, SO_x, H_2S, NO_x, NH_3 and fine particle matter (PM_{10} and $PM_{2.5}$) are pollutants and among the major environmental threats to human health. Prevention and control of air pollution still represent the main challenges for modern society. At the same time, these pollutants cause climate change and negatively affect the natural biogeochemical cycles of many elements.[7]

Realizing the gravity of the problems, researchers have developed several techniques to remove SO_2 and H_2S from gaseous emissions and mixtures. Previous studies have considered alkaline aqueous solutions and alkylamine solutions to

[a] *University of Belgrade, Institute of Chemistry, Technology and Metallurgy, National Institute of Republic of Serbia, Njegoševa 12, Belgrade, 11000, Serbia. E-mail: sonja.grubisic@ihtm.bg.ac.rs*
[b] *Université Gustave Eiffel, COSYS/IMSE, 5 Bd Descartes 77454, Champs sur Marne, France. E-mail: majdi.hochlaf@univ-eiffel.fr*
[c] *University of Tunis El Manar, Department of Chemistry, Laboratory of Characterizations, Applications and Modeling of Materials (LCAMM), LR18ES08, Tunis, Tunisia*

† Electronic supplementary information (ESI) available. See DOI: https://doi.org/10.1039/d2cp04295a

‡ Present address: Université Paul Sabatier Toulouse [UT3], Laboratoire de Chimie Physique Quantiques (LCPQ), Fédération Fermi, UMR 5626, CNRS, 118 Route de Narbonne, 31062 Toulouse, France.

capture sulphur gases.[8,9] The more efficient procedures for capturing sulphur bearing gases included ozone injection[10] and organic superbases of a tertiary amine.[11] Some recent approaches successfully implemented liquid-based adsorbents for SO_2 and H_2S removal. Liquid-based adsorbers containing ammonium or imidazolium salts influence the conversion of SO_2, higher than 95% at a relatively low working temperature of 40 °C and with good recycling.[12,13] The need for using water or organic solvents in these procedures is a drawback due to increased liquid waste. Therefore, scientific attention has shifted towards dry adsorption procedures of removing sulphur gases with porous materials such as zeolites[14–16] and metal–organic framework materials (MOFs).[7,17,18] Besides, metal oxides,[19–22] porous materials, activated carbons,[23–25] and carbon nanotubes[26] have shown efficient capture ability for acids and other gases. In particular, MOFs have been recognized as promising materials for gas capturing due to their cavity dimension, the diversity of their chemical composition, the possibility of ligand functionalization, and the relatively low-cost reactivation.[27,28]

In the literature, only a few theoretical and experimental studies on the H_2S and SO_2 removal by MOFs have been published.[29–34] Most of them are recent. Indeed, experimental and computational efforts have been made recently to explore the use of MOFs[35] or natural or synthetic zeolites[36] for the effective removal of SO_2 and H_2S gases. For instance, Xu *et al.*[31] conducted an experimental study on ZIF8 functionalized with aminoterazole ATZ (*i.e.*, ZIF8-A), confirming that the introduction of amino groups enhances the SO_2 adsorption capacity due to the formation of hydrogen bonds between SO_2 and these amino groups. They also established a SO_2 saturation capacity of 498 mg g^{-1} and 336 mg g^{-1} for ZIF8-A and ZIF8, respectively. Furthermore, the SO_2 saturation capacity of ZIF8-A/*n*-heptanol (589 mg g^{-1}) was 18.3% higher than that of ZIF8-A under the same experimental conditions. Very recently, Wang *et al.*[32] reported a combined theoretical and experimental study of reversible SO_2 adsorption by ZIF8 modified with 5-aminotetrazole (*i.e.*, $Zn(5\text{-}ATZ)_{1.5}$). They showed that the SO_2 adsorption capacity of $Zn(5\text{-}ATZ)_{1.5}$ at a concentration of 1.6% vol can reach 122 mg g^{-1} under optimal conditions. Within the $Zn(5\text{-}ATZ)_{1.5}$ pores, SO_2 interacts *via* hydrogen bonds between its oxygens and the amino hydrogen of the $Zn(5\text{-}ATZ)_{1.5}$ or with the nitrogen of 5-amino tetrazole forming a non-covalent charge transfer complex. Moreover, theoretical study by Zhou *et al.*[33] explored the selectivity and adsorption capacity of various zeolitic imidazolate frameworks towards H_2S and SO_2 gases. In particular, they showed that UiO-66, ZIF-71, ZIF-69, and ZIF-97 exhibit good performances for H_2S separation from air, with selectivity and adsorption capacities higher than 300 mg g^{-1} and 0.01 mmol g^{-1} at room temperature and atmospheric pressure, respectively. Besides, Beheshti *et al.*[34] synthesized a set of four new sulphur coordination polymers (*e.g.* $[ZnCl_2(L_s)_2]_n$ polymer where the ligands L_s = 1,1′-(pentane-1,5-diyl)bis(-3-methyl-1*H*-imidazole-2-thione)). They pointed out the high adsorption capacity of these polymers, which is due to the hydrogen bonding interactions between the H_2S molecules and the neighboring flexible sulphur donor linker, chloride, thiocyanate, and uncoordinated perchlorate anions. Furthermore, Song *et al.*[37] reported through computational study with grand canonical Monte Carlo (GCMC) simulation combined with DFT that SO_2 interacts with MOF IRMOF10 (M = transition metal = Zn) first, through Zn atoms since they are more energetically favorable as adsorption sites, then through H bonds of organic unit *i.e.* C–H groups. As a general outcome, the studies confirmed that MOFs containing N-heterocycles improved SO_2 adsorption and emphasized the importance of modulating the host–guest binding interaction between gases (H_2S and SO_2) and MOFs to achieve a reversible process.[7] In sum, these previous works showed that zeolites, as adsorbents, interact with acid gases through chemosorption (covalent bonds), which generate an irreversible structure transformation, whereas MOFs interact with guest molecules through physical or weak chemical adsorption which requires a lower energy cost regeneration without transforming the adsorbent structure.[35]

Molecular simulation techniques have been proven to be more cost-efficient alternatives to experimental investigations of the influence of different factors such as the diameter and surface of the pores, pressure, temperature, and nature of the MOF–gases interactions. However, the capture of acidic gases such as H_2S and SO_2 by MOFs has been demonstrated to be a difficult and challenging task, mainly due to the formation of a strong and sometimes irreversible bond (*e.g.*, a metal–sulphur bond in the case of H_2S), causing structural degradation of MOFs.[38,39] Consequently, the type of interaction between the host and guest plays a key role in order to achieve a good adsorption capacity with low cost regeneration of adsorbents. Accordingly, we need to regulate (or to adjust) the type of binding interaction through several types of adsorbents. Indeed, the determination of appropriate host–guest binding interactions between MOFs and H_2S or SO_2, such as non-covalent interactions, hydrogen bonds, or donor-acceptor bonds, is a decisive factor for successful reversible sulphur gas capture.

Recently, we have presented an *in silico* method to design a new MOF, named ZTF (for the zinc triazolate based framework), exhibiting good adsorption properties for CO_2 capture.[40] The newly designed ZTF MOF was generated by replacing the NH_2 group of the triazolate ring of the MAF-66 MOF[40] with a hydrogen atom. Our initial DFT investigations of the stable structures of the non-reactive and reactive clusters formed between Zn^{2+}-triazole ([Zn^{2+}-Tz]) and CO_2 and/or H_2O, where [Zn^{2+}-Tz] is the subunits of triazolate based MOFs, showing the presence of covalent or weak interactions (hydrogen bonds, van der Waals type) between the [Zn^{2+}-Tz] subunits and CO_2 and/or H_2O molecules.[41,42] We have further studied the carbon dioxide and water adsorption in both ZTF and MAF-66 zinc triazolate based frameworks by using force field based GCMC simulations. GCMC simulations indicated that the ZTF MOF has a higher CO_2 adsorption capacity than MAF-66 at high pressure under dry conditions, at 273 K. This sequestration is associated with the formation of several types of interactions such as electron acceptor–electron donor interactions between the

carbon of CO_2 and the nitrogen of triazole (Tz) of ZTF, π stacking interactions between CO_2 and aromatic rings of Tz and hydrogen bonds. In addition, the results showed that strong hydrogen bonds between water molecules and N atoms of Tz rings are responsible for water adsorption in MAF-66 and ZTF structures. Furthermore, adsorption is favored by Lewis acid–Lewis base interactions, and hydrogen bonds, along with electrostatic interactions. The good performances of our MOF model (ZTF) for CO_2 uptake inspired us to further investigate toxic or corrosive gases that must be removed from the atmosphere such as SO_2 and H_2S.

In the search for new alternatives for capturing SO_2 and H_2S pollutants, here we have investigated the adsorption of SO_2 and H_2S, with and without the presence of H_2O/CO_2 molecules by both MAF-66, a well-established high gas capture MOF, and ZTF MOF using the GCMC and first principles approaches. Through comparison of the ZTF and MAF-66, we target testing the adsorption properties of our recently proposed ZTF porous material to enhance the adsorption capacity of MOFs and to predict new alternatives of these materials for H_2S and SO_2 capture under dry and humid conditions. At the microscopic level, we found several binding sites between ZTF/MAF-66 and pollutant guest molecules through weak interactions (hydrogen bonds, van der Waals). In addition, metal–organic frameworks such as those considered in this work are a class of materials consisting of zinc metal ions that remain joined together through organic linkers, leading to the formation of three dimensional structures. Hence, their properties and applications are closely related to those of zinc cluster subunits themselves, and more generally, zinc metal clusters. In this way, our GCMC simulations were carried out using $3 \times 3 \times 3$ supercell models including more than 200 Zn atoms inside.

II. Computational details

Our computations started with periodic density functional theory (DFT) calculations using the SIESTA[43,44] software package, with the generalized gradient approximation (GGA) of the PBE functional.[45] Double zeta polarized basis sets (DZP) and norm conserving pseudo potentials have been used for these computations.[46] DFT calculations consist of optimizing the structures of MAF-66 and ZTF positions, together with H_2S and SO_2 molecules inside the pores. Real space integrals are performed on a mesh with a 200 Ry cut-off. Geometry optimizations were performed in such a way to allow full atomic and cell relaxation without geometrical constraints up to a force threshold of 0.05 eV $Å^{-1}$. The Brillouin zone was sampled by the $4 \times 4 \times 4$ Γ-centered Monkhorst–Pack k-point.

Adsorption energies (ΔE_{ads}) for SO_2 and H_2S molecules are calculated using the following equations:

$$\Delta E_{ads} = E_{Zc} - (E_{MOF} + E_X) \quad (1)$$

where X refers to SO_2 or H_2S; E_{Zc} represents the total energy of ZTF or MAF-66 with the adsorbed guest molecules SO_2 or H_2S; E_{MOF} corresponds to the total energy of this MOF solely. E_X is the total energy of the isolated H_2S or SO_2 molecules evaluated using a supercell with dimensions of $10 \times 10 \times 10$ Å. Attractive interactions correspond to negative values of ΔE_{ads}, which means a thermodynamically favored SO_2 or H_2S binding to the MOF pore surface.

The interaction energy between the atoms was computed through Lennard–Jones (LJ) potentials. This LJ potential is a simple pair potential, representing the London dispersion forces that can accurately model weak van der Waals bonds and has the following form:

$$V_{ij} = 4\varepsilon_{ij}\left[\left(\frac{\sigma_{ij}}{r_{ij}}\right)^6 - \left(\frac{\sigma_{ij}}{r_{ij}}\right)^{12}\right] \quad (2)$$

where r_{ij} is the distance between interacting atoms i and j; ε_{ij} and σ_{ij} are LJ potential parameters *i.e.* the well depth and diameter at which the intermolecular potential between the two particles is zero, respectively.

In this work, the standard combining rules of Lorentz–Berthelot were considered to estimate the cross terms of the LJ parameters. LJ parameters for all atoms of frameworks were taken from the DREIDING[47] force field supplemented with zinc parameters from the Universal Force Field.[48] These parameters are listed in Table 1 together with the partial charges, which are deduced from DFT calculations. The listed DFT partial atomic charges of ZTF and MAF-66 were validated in our previous work.[40] For those of SO_2 and H_2S, we used a similar calculation scheme. Moreover, CO_2, SO_2 and H_2S were modelled as three-site rigid molecules with charges on each site. Partial charges and LJ parameters for CO_2, SO_2 and H_2S were taken from the TraPPE[49–52] force field and are listed in Table 1 as well. The parameters used to model SO_2 and H_2S are able to reproduce the bulk phase properties of these species.[51,52] They have been widely used to investigate adsorption in porous carbons, zeolites and MOFs.[52,53] For the studies of the water adsorption in ZTF, the TIP3P[54] model was selected for H_2O molecules. Lorentz-Berthelot mixing rules were employed to calculate cross-LJ interactions.

Monte Carlo simulations were used to compute the single adsorption isotherms of SO_2 and H_2S in MAF-66 and ZTF. Besides, we have examined the adsorption of SO_2 and H_2S in the presence of H_2O or CO_2 molecules. All simulations were performed with the Monte Carlo[55] suite of the RASPA code.[56] A cut-off distance of 12 Å was used for LJ interactions. The Ewald sum technique was used to complete the electrostatic interactions. Simulations were performed using $3 \times 3 \times 3$ supercells and included random insertion, abstraction and translation motions of molecules with equal probabilities. The simulations consisted of 3×10^5 equilibrations and 6×10^5 production cycles.

The void fraction of each MOF structure was determined in the GCMC simulations using spherical probes that were representative of He atoms. These GCMC simulations were carried out on PARADOX-IV supercomputing facility.

Table 1 Force field parameters of guest molecules (SO_2, H_2S, CO_2, and H_2O) and of [Zn-Atz] and [Zn-Tz] which are subunits of MAF-66 and ZTF used in GCMC simulations. ε/k_b (K), σ (Å) and q (e) correspond to Lennard–Jones potential parameters and atomic partial charges. The numbering of atoms is also given

SO_2		Atom	O	S		H_2S		Atom	S	H		
		ε/k_b	62.3	154.4				ε/k_b	250.0	3.90		
		σ	2.99	3.58				σ	3.72	0.98		
		q	−0.235	0.470				q	−0.248	0.124		
CO_2		Atom	O	C		H_2O		Atom	O	H		
		ε/k_b	79.0	27.0				ε/k_b	76.542	7.649		
		σ	3.05	2.80				σ	3.15	2.846		
		q	−0.35	0.70				q	−0.834	0.417		
[Zn-Atz]		Atom	Zn1	N1	N2	N3	N4	C3	C5	H3A	H3B	H3C
		ε/k_b	62.399	38.149	38.149	38.149	38.149	47.856	47.856	7.649	7.649	7.649
		σ	2.4615	3.2626	3.2625	3.2626	3.2626	3.473	3.473	2.846	2.846	2.846
		q	1.108	−0.33	−0.33	−0.35	−0.35	0.0059	0.0059	0.08	0.08	0.08
[Zn-Tz]		Atom	Zn1	N1	N2	C3	N4	C5	H3A	H3B		
		ε/k_b	62.399	38.149	38.149	47.856	38.149	47.856	7.649	7.649		
		σ	2.4615	3.2626	3.2626	3.4730	3.2626	3.2626	2.846	2.846		
		q	1.118	−0.396	−0.396	0.0059	−0.398	0.0059	0.03	0.03		

III. Results and discussion

A. Structural and adsorption energy calculations

First principles DFT calculations were used to optimize the structures of SO_2 and H_2S inside the pores of MAF-66 and ZTF MOFs and to evaluate the energetics associated with the adsorption of SO_2 and H_2S molecules at the surface of the pores of MAF-66 and ZTF frameworks. Optimized structures of MAF-66 and ZTF with SO_2 and H_2S molecules inside cavities are presented in Fig. 1. In the case of ZTF we performed calculations for 2 initial positions of SO_2 and H_2S. Optimized structures of ZTF with SO_2 and H_2S molecules inside cavities are shown in Fig. 2 and 3, respectively. We give in Table 2 the structural parameters of optimized MOFs (MAF-66 and ZTF) with H_2S or SO_2 inside the pores. The results are similar to those discussed in ref. 40 as well as the experimental geometrical parameters for the MAF-66 crystal structure given by Lin *et al.*[57] The calculated volumes inside the MOFs available for adsorption are 1329 Å^3 for MAF-66 and 1383 Å^3 for ZTF. The computed pore sizes are 0.45 and 0.50 nm for MAF-66 and ZTF. The helium void fraction and the surface area were computed with RASPA and they are the same as those given in ref. 40. The structural parameters of these empty MOFs did not change upon insertion of H_2S/SO_2 gases inside their pores due to the formation of reversible non-bonded weak interactions between such guest molecules and the respective surface pores.

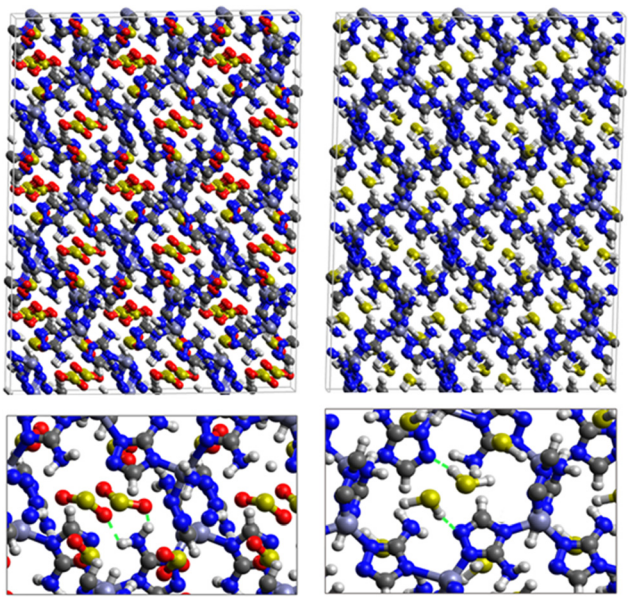

Fig. 1 Top: DFT optimized 3D structures of SO_2 (left) and H_2S (right) inside MAF-66. Bottom: Enlargement in the vicinity of SO_2 and H_2S molecules where non-bonded interactions are also shown with green dashed lines.

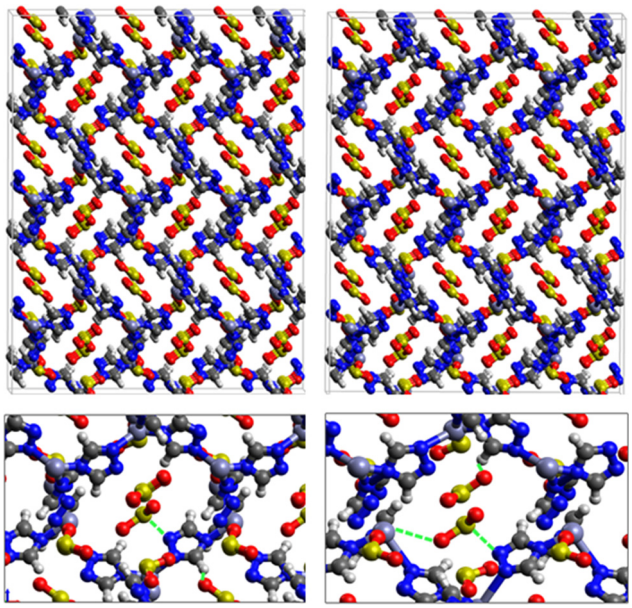

Fig. 2 Top: DFT optimized 3D structures of SO_2 inside ZTF with binding energies of −7.48 kcal mol^{-1} (left) and of -9.00 kcal mol^{-1} (right). Bottom: Enlargement in the vicinity of SO_2 molecules where non-bonded interactions are also shown with green dashed lines.

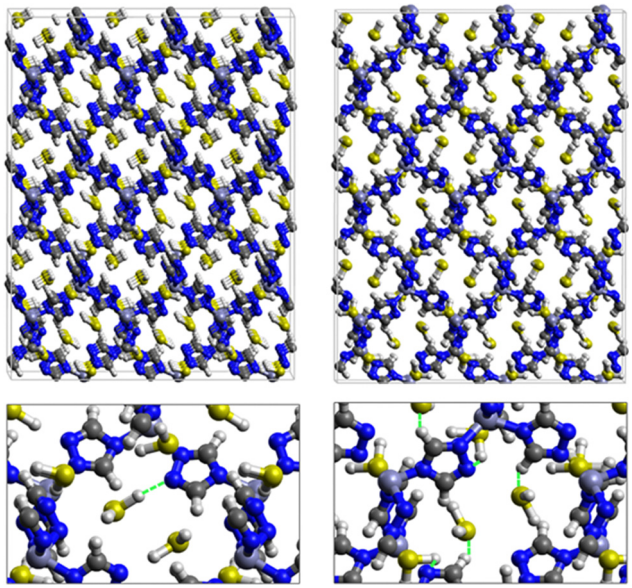

Fig. 3 Top: DFT optimized 3D structures of H_2S inside ZTF with binding energies of −13.5 kcal mol^{-1} (left) and of −7.41 (right). Bottom: Enlargement in the vicinity of H_2S molecules where non-bonded interactions are also shown with green dashed lines.

Fig. 1 shows that SO_2 molecules are adsorbed in MAF-66 through H-bonds between O atom of SO_2 and H atom of amino group (NH_2), whereas inside ZTF the main interactions that contribute to the adsorption mechanism are between the positively charged S atom of SO_2 and the uncoordinated N atom or between the O atom of SO_2 and zinc of ZTF pore classified as electrostatic interactions (Fig. 2). For H_2S inside MAF-66 and ZTF MOF pores, the present DFT calculations showed that the principal interactions between H_2S and surface pores involves the nitrogens of this nanomaterial through a relatively strong hydrogen bonds (Fig. 1 and 3) and between sulfur of H_2S bonded to H–C of Tz (Fig. 3).

We have calculated adsorption energies (ΔE_{ads}) of one SO_2/H_2S molecule inside MAF-66 or ZTF pores and for 2 different positions of sulfur gases inside MOFs using the procedures described above. Table 2 shows that the calculated adsorption energies of SO_2 inside MAF-66 and ZTF are −11.41 and −7.48/−9.0 kcal mol^{-1}, respectively. Adsorption energies of H_2S inside MAF-66 and ZTF are slightly larger. Indeed, they amount to −11.56 and −13.50/−7.41 kcal mol^{-1}. The binding energies are in the range of physical adsorption. When hydrogen sulfide is adsorbed only *via* hydrogen atom of H_2S, the binding energy of this configuration is slightly lower than the configuration when sulfur atom of H_2S is included in adsorption (Fig. 3). Similar mechanism of adsorption of H_2S inside MAF-199 was already noticed.[58] Therefore, both MAF-66 and ZTF nanoporous materials favor the adsorption of sulfur dioxide and hydrogen sulfide molecules, mainly due to the interactions between these guest molecules and the functional groups available at the surface of the corresponding pores. Besides, the adsorption of H_2S is slightly stronger than that of SO_2 because of the H-bonding interactions described above. They are indeed the main driving forces for the high adsorption capacities of ZTF and MAF-66. This is in line with our previous investigation of water inside a ZTF MOF, where we concluded that the H bonding interactions of water molecule guests with N atoms of ZTF dominate their adsorption properties and therefore enhance their performances, in particular at low pressures.[40]

B. GCMC simulations

a. Adsorption of SO_2 and H_2S inside MAF-66 under dry conditions. GCMC simulations have been performed using the DFT optimized structure of MAF-66. The simulated adsorption isotherms for pure SO_2 and H_2S gases inside MAF-66 at temperatures of 273 K and 298 K are presented in Fig. 4. The adsorption isotherms of both gases exhibit Type-I adsorption isotherms,[56] where the shape is due to attractive adsorbate–adsorbent forces. Similar adsorption results were observed in our previous study with CO_2 as the guest molecule.[40] As can be seen from Fig. 4, the simulated isotherms for SO_2 adsorption reaches saturation at 0.1 atm at both 273 K and 298 K temperatures. The simulated SO_2 uptake of MAF-66 at 1 atm and at 273 K and 298 K are equal to ∼223 cm^3 (STP) cm^{-3} (150 cm^3 (STP) g^{-1}) and ∼218 cm^3 (STP) cm^{-3} (147 cm^3 (STP) g^{-1}), respectively. For H_2S the average absolute adsorption values at 273 K and 298 K are equal to ∼ 220 cm^3 (STP) cm^{-3} (148 cm^3 (STP) g^{-1}) and ∼200 cm^3 (STP) cm^{-3} (134 cm^3 (STP) g^{-1}). Uptake of SO_2 at lower pressure in MAF-66 is higher than H_2S for both temperatures due to the stronger non-bonded interactions of SO_2 and pore surface atoms.

Fig. 5 shows the adsorption positions of SO_2 and H_2S molecules inside the pores of MAF-66 after GCMC

Table 2 Unit cell parameters (a, b, and c in Å and α, β, and γ in degrees), volume of MOFs (vol in Å^3) and adsorption energies per molecule (ΔE_{ads} in kcal mol^{-1}) for adsorption of SO_2 or H_2S inside MAF-66 and ZTF as calculated with SIESTA. We give also the average bond lengths (in Å) and angles (in degrees) of guest molecules of DFT optimized structures. In parentheses are data for another configuration of SO_2 and H_2S inside ZTF (see text)

								SO_2			H_2S		
MOF	a	b	c	α	β	γ	Vol	ΔE_{ads}	Bond	Angle	ΔE_{ads}	Bond	Angle
MAF-66	9.939	10.076	13.287	91.6	88.5	88.8	1329	−11.41	1.485	118	−11.56	1.361	91
ZTF	10.25	10.22	13.20	90.7	89.9	89.6	1383	−7.48	1.548	113	−13.50	1.485	95
	(10.25)	(10.23)	(13.21)	(90.7)	(89.9)	(89.6)		(−9.00)	(1.517)	(116)	(−7.41)	(1.388)	(90.4)

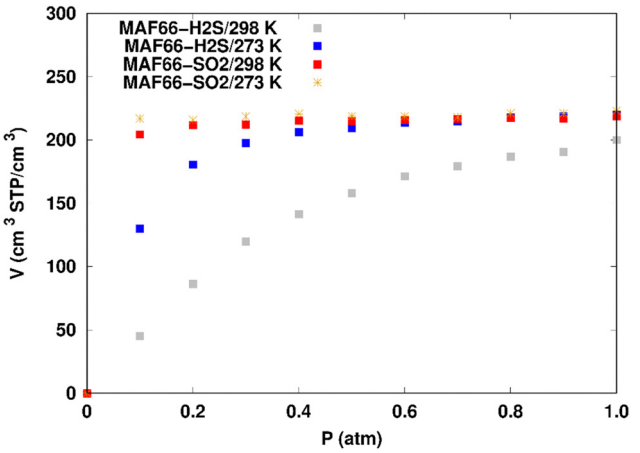

Fig. 4 Simulated adsorption isotherms of SO_2 and H_2S in MAF-66 at 273 and 298 K.

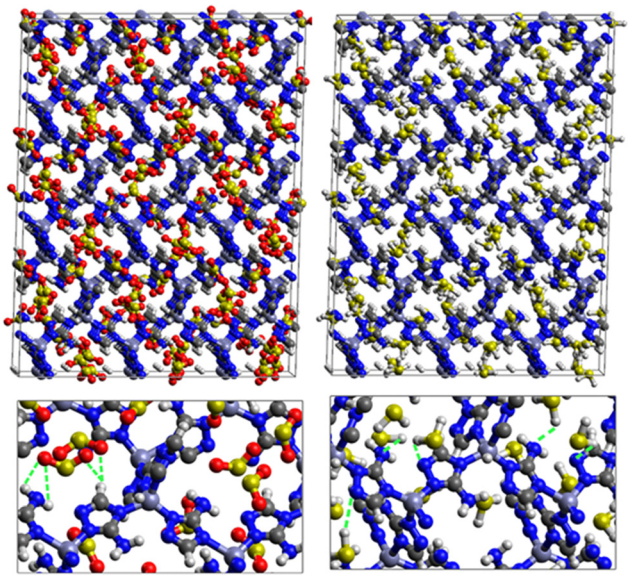

Fig. 5 Top: GCMC adsorption sites of SO_2 (left) and H_2S (right) molecules inside the pores of MAF-66. Bottom: Enlargement in the vicinity of SO_2 and H_2S molecules where non-bonded interactions are also shown.

computations, together with non-bonded interactions between adsorbed hosted molecules and pores. SO_2 is adsorbed on the surface of the MAF-66 pore by two types of hydrogen bonds, either between one oxygen of SO_2 with the closest hydrogen of the triazole 5-membred ring or between one oxygen of SO_2 with the hydrogens of the amino group. These interactions depend on the orientation of SO_2 inside the pore. In the case of H_2S, GCMC simulations reveal that H_2S interacts with MAF-66 mainly through hydrogen bonds between the nitrogens of the MOF organic subunit and the hydrogens of H_2S. The same interactions between sulfur containing gases and MAF-66 are found at first and middle snapshots extracted during GCMC simulations (see Fig. S1 and S2, ESI†).

b. Adsorption of SO_2 and H_2S inside ZTF. GCMC simulations were carried out to calculate the SO_2 and H_2S adsorption isotherms in ZTF at 273 K and 298 K. Simulated adsorption isotherms are presented in Fig. 6. Again, the adsorption isotherms of both gases exhibit a Type-I adsorption isotherm, where the shape is due to attractive adsorbate–adsorbent forces. Fig. 6 shows that SO_2 adsorption reaches saturation at 0.1 atm at both temperatures. The simulated SO_2 uptake of ZTF at 1 atm and 273 K is equal to ∼231 cm^3 (STP) cm^{-3} (180 cm^3 (STP) g^{-1}) while for H_2S the average absolute adsorption value is equal to ∼208 cm^3 (STP) cm^{-3} (162 cm^3 (STP) g^{-1}) under similar conditions. As for MAF-66, the uptake of SO_2 is slightly decreased at higher temperature. This is in line with the findings of Wang *et al.*[32] who investigated the influence of

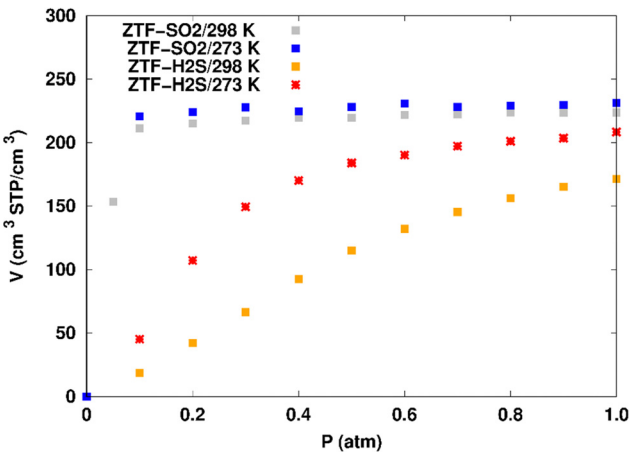

Fig. 6 Simulated adsorption isotherms of SO_2 and H_2S in ZTF at 273 and 298 K.

temperature in the range of [25–65] °C on the adsorption uptake of Zn(5-ATZ) and showed that the adsorption capacity of SO_2 decreases as the adsorption temperature increases suggesting that the interaction between Zn(ATZ) is weak.

Fig. 6 shows that the uptake of H_2S is lower than SO_2 for both temperatures. Nevertheless, the differences between ZTF and MAF-66 MOFs for both guest molecules remain small (Fig. 4 and 6). The SO_2 saturation capacity of ZTF is equal to $\sim$515 mg g^{-1} at 273 K and $\sim$500 mg g^{-1} at 298 K. This capacity is 48.2% higher than that of ZIF8 (336 mg g^{-1}) and similar to ZIF8-A (498 mg g^{-1}) at T = 298 K,[31] suggesting the good performance of our proposed model. In addition, the SO_2 saturation capacity of Zn(5-ATZ) is 122 mg g^{-1} (for a specific surface area of 386 m^2 g^{-1}) which is slightly lower than ZIF8-A if we compare their adsorption capacity considering the same specific surface area where SSA ZIF8-A $\sim$3 SSA Zn(5-ATZ). In the case of H_2S, the saturation capacity of ZTF is $\sim$246 mg g^{-1} at 273 K and $\sim$202 mg g^{-1} at 298 K, which is acceptable comparing to other adsorbents with high performance ($\sim$300 mg g^{-1}).[33]

Fig. 7 displays the adsorption positions of SO_2 and H_2S molecules inside the pores of ZTF after GCMC simulations, together with non-bonding interactions between adsorbed hosted molecules and pores. The GCMC snapshots of initial and middle frames are also presented in Fig. S3 and S4 (ESI†). The SO_2 molecules are stabilized in the pores of ZTF by several types of interactions: either by the hydrogen bonds between one oxygen of SO_2 and the hydrogen of the C–H of the triazole organic subunit or by the electrostatic interactions between the nitrogens of the MOF subunit and the sulphur of SO_2 or by the electrostatic interaction between metal zinc of these MOFs and oxygens of SO_2. It has been found that the SO_2 molecule electrostatically orients to the unsaturated coordination sites (which act as M$\cdots$O(SO_2) acid–base Lewis interactions), and hence SO_2 is physisorbed rather than chemisorbed. Thus, the collapse of the MOF structure is avoided. Similar interactions were already observed.[7,37] For example, in IRMOF-10 MOFs, Song *et al.*[37] suggested that the SO_2 molecules initially occupy the zinc corner regions through Zn$\cdots$O(SO_2) electrostatic interactions, as the most favorable energetic adsorption sites. These authors also found weak hydrogen bonds between the aromatic C–H group and O of SO_2. In the case of H_2S, we identified the presence of hydrogen bonds between the hydrogens of H_2S and the nitrogens of Tz subunits. It was also observed that increasing temperature had an adverse effect on H_2S adsorption as can be seen in Fig. 4 and 6, suggesting that physical adsorption is predominant. In addition to this, as already pointed out in ref. 35 and 37, pore sizes greater than 0.4 nm have high SO_2/H_2S gas adsorption capacity and the volume/surface area are still important characteristics for evaluating gas adsorption potential.

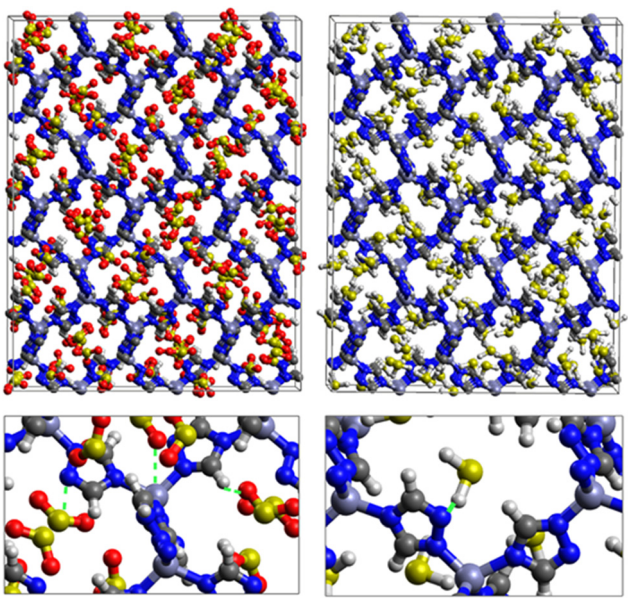

Fig. 7 Top: GCMC adsorption sites of SO_2 (left) and H_2S (right) molecules inside the pores of ZTF. Bottom: Enlargement in the vicinity of SO_2 and H_2S with non-bonded interactions are also presented.

c. Co-adsorption of SO_2 and H_2S besides H_2O and CO_2 inside ZTF. The effect of water on the adsorption of sulfur gases inside ZTF was considered as follows: the water molecules were introduced at two active sites in ZTF such as the coordinately unsaturated Zn atoms and the uncoordinated N atom of the triazolate ring. Initial structures of ZTF with the addition of H_2O molecules used for GCMC simulations were optimized using DFT calculations. They are shown in Fig. 6 of ref. 40. In addition to this, simulations with preloaded water molecules (up to 100 water molecules) were also performed.

In the case of carbon dioxide, we considered the adsorption of SO_2 and H_2S with N_{CO_2} preloaded CO_2 molecules (SO_2–CO_2 and H_2S–CO_2 mixtures). While the number of SO_2 and H_2S molecules varied in the course of simulations, the number of CO_2 molecules was kept fixed to N_{CO_2}. Also, CO_2 molecules were allowed to move within the cavities of these MOFs until reaching equilibrium.

SO_2 adsorption in ZTF with active sites occupied by H_2O molecules. We performed GCMC simulations to evaluate the SO_2 adsorption isotherms for the hydrated ZTF MOF at 298 K. Here, we report the GCMC results of the influence of the H_2O molecules on SO_2 adsorption where water molecules occupy either the coordinately unsaturated Zn atoms or the uncoordinated N atom of the triazolate ring active sites. The corresponding simulated adsorption isotherms of SO_2 at 298 K in ZTF with and without the presence of H_2O molecules in two different positions are shown in Fig. 8. This figure reveals that SO_2 uptake significantly decreases when H_2O molecules are located in the vicinity of the nitrogen of the triazole subunit. Indeed, when going from dry to hydrated conditions at higher pressures (P $\sim$ 1 atm) the average absolute adsorption values of SO_2 significantly decreased from $\sim$223 cm^3 (STP) cm^{-3} to $\sim$168 cm^3 (STP) cm^{-3} when H_2O interacts with nitrogen through N$\cdots$H(OH) hydrogen bond. Whereas, when H_2O molecules are placed near the Zn atom, the situation is different, where the presence of water molecules slightly changes the adsorption of SO_2 from 220 cm^3 (STP) cm^{-3} to 219 cm^3 (STP) cm^{-3}. In fact, humidity in MOF materials with open metal sites has unfavorable effects on the capture of SO_2 due to the competition between this molecule and water molecules

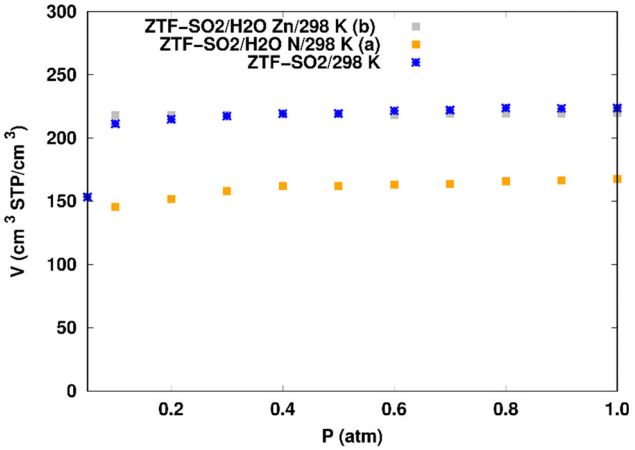

Fig. 8 Simulated adsorption isotherms of SO_2 at 298 K in ZTF with and without the presence of water molecules, where H_2O is located near a nitrogen of the surface pore (in (a)) or in the vicinity of the Zn atom (in (b)).

towards the interactions with the nitrogens or open metal sites which are possible sites for SO_2 adsorption through electrostatic $SO_2\cdots N$ and $M\cdots O$ (SO_2) interactions (Fig. 9). Similar behavior of an unfavorable effect of humidity on the capture of SO_2 while using Mg-MOF-74[7] as the MOF is also observed as well in our previous work with CO_2 as guest molecule inside ZTF.[40]

Fig. 9 shows the GCMC adsorption sites of SO_2 molecules inside the pores of ZTF in the presence of H_2O molecules near the zinc or nitrogen atoms of the [Zn-triazole] subunits. Close examination of this figure reveals the occurrence of several types of interactions that contribute to the SO_2 capture by the MOF. Again, when water is near the nitrogens several types of interactions were found: (i) hydrogen bonds between one oxygen of SO_2 and the hydrogen of triazole subunit (*i.e.* C–H–O(SO_2)), with d{O_{SO_2}–H_C} distances in the [2.8–3.0] Å range. (ii) Electrostatic interactions between one oxygen of SO_2 and the zinc atom of the [Zn-triazole] subunit with d{O_{SO_2}–Zn_{Tz}] in the ∼[3.09 – 3.3] Å range. (iii) Hydrogen bonds between the hydrogen of H_2O and the unprotonated nitrogen of Tz, N–H(H_2O), with d{H_{H_2O}–N} distances in the [1.8–2.2] Å range.

When H_2O is placed near the zinc of the [Zn-triazole] subunit, the electrostatic interaction is present between the oxygen of water and the zinc of Tz with intermolecular distances of ∼[2.3–2.4] Å. Also, we found π stacking interactions between the SO_2 molecule and the aromatic ring of the triazole subunits, as well as electrostatic interactions between one oxygen of SO_2 and the unprotonated nitrogen of triazole with d{O_{SO_2}–N_{Tz}} in the ∼[2.75–3.1] Å range. In addition, we characterized hydrogen bonds between the oxygen of SO_2 and the hydrogen of triazole, C–H–O(CO_2), with d{O_{SO_2}–H_C} distances in the [2.65–3.3] Å range. These types of interactions (H-bonds and electrostatic) were also identified between CO_2 and the surface pore atoms of ZTF.[40] Consequently, the selectivity of MOFs towards adsorbents for the CO_2/SO_2 gas mixture should be challenging. Nevertheless, ZTF exhibits a better binding affinity to SO_2 compared to CO_2 due to the polar character of SO_2, which induces the stabilizing electrostatic interactions highlighted above. For instance, the average absolute adsorption value of CO_2 in ZTF at 273 K and 1 atm, is equal to ∼174 cm^3 (STP) g^{-1} [40] and of SO_2 is equal to ∼180 cm^3 (STP) g^{-1} under the same P and T conditions.

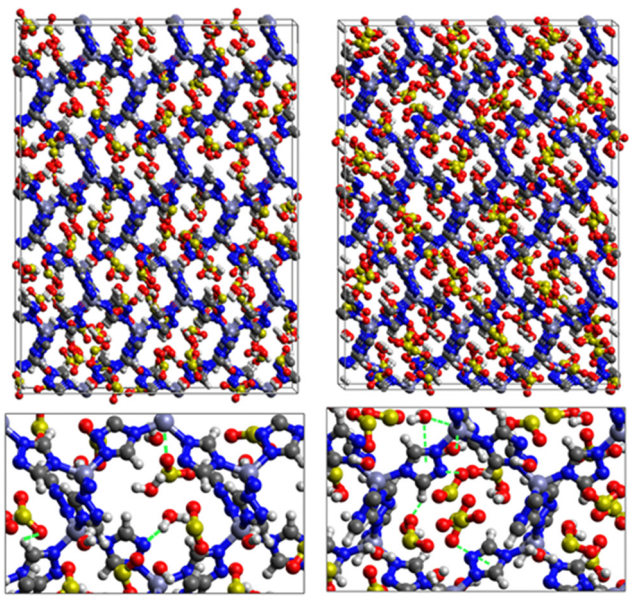

Fig. 9 Top: GCMC adsorption sites of SO_2 molecules inside the pores of ZTF in the presence of H_2O near the nitrogen atom of the triazole subunits (left) or near the Zn atom (right). Bottom: Enlargement in the vicinity of SO_2 and H_2O where non-bonded interactions are also highlighted.

H_2S adsorption in ZTF with active sites occupied by H_2O molecules. GCMC simulations were performed to investigate the H_2S adsorption isotherms for a hydrated ZTF MOF at 298 K. The corresponding simulated adsorption isotherms with and without the presence of water molecules are shown in Fig. 10. This figure allows us to identify two regimes:

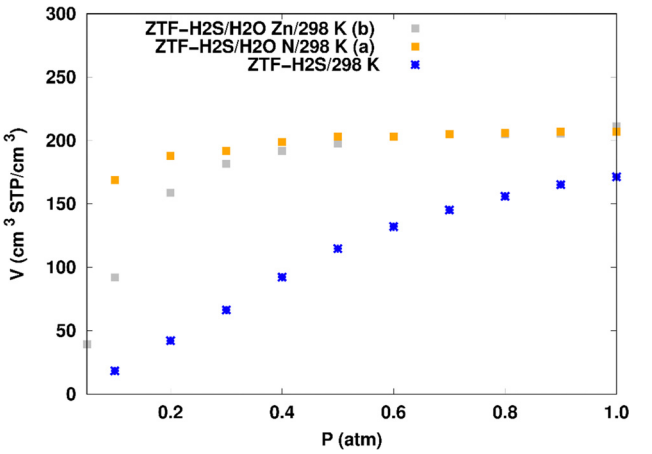

Fig. 10 Simulated adsorption isotherms of H_2S at 298 K in ZTF with and without the presence of water molecules, where H_2O is located near nitrogen (in (a)) or in the vicinity of the Zn atom (in (b)).

(i) "very low pressure" regime for $P < 0.3$ atm: dry ZTF presents lower capacities for H_2S uptake than the hydrated case. The enhancement of adsorption is better when water is placed near nitrogen. For instance, H_2S uptake significantly increases from 42.08 cm^3 (STP) cm^{-3} at $P = 0.2$ atm and $T = 298$ K under dry conditions to 188.0/158.78 cm^3 (STP) cm^{-3} in the presence of water. Thus the presence of H_2O molecules attached to both adsorption sites (around Zn and at N of triazole) enhances the H_2S adsorption.

(ii) "high pressure" regime for $P > 0.3$ atm: we observe an identical increase in H_2S adsorption for both positions of water inside pores. The position of water seems not to have any difference on the H_2S uptake. Indeed, a plateau is observed at around 211.0 cm^3 (STP) cm^{-3}. This is the signature of a saturation of the H_2S adsorption available sites. Fig. 10 also shows that the H_2S uptake slightly increases when H_2O molecules are present for higher pressures. For instance, H_2S uptake slightly increases from 170.1 cm^3 (STP) cm^{-3} at $P = 1$ atm and $T = 298$ K under dry conditions to around 211 cm^3 (STP) cm^{-3} in the presence of water. Such water induced enhancement of H_2S adsorption on nanomaterials was already experimentally observed.[7]

Nonbonded interactions between H_2S and ZTF pore are presented in Fig. 11. In this case, we observe hydrogen bonds between the hydrogen of C–H with sulfur of H_2S for both positions of water. We also characterized interaction between the hydrogen of triazole and sulfur of H_2S C–H–S(H_2S), with d{S_{SO_2}–H_C} distances in the [2.7–3.5] Å range.

SO_2/H_2S adsorption with a fixed number of preloaded H_2O molecules inside the ZTF pore. We performed several simulations where we varied the number of preloaded H_2O molecules (N_{water}) inside the ZTF cavity. Table 3 gives the results of the SO_2 and H_2S adsorption in the ZTF model MOF by varying N_{water} from 0 to 100. All simulations were performed at a temperature of 273 K and at very low (0.1 atm) and high pressures (1 atm). Table 3 shows that, at both pressures, increasing the number of H_2O molecules up to 10 slightly increases the amount of adsorbed SO_2 (at 0.1 atm from ~221 to ~224 cm^3 (STP) cm^{-3}). Beyond this preloaded amount of H_2O, the SO_2 uptake starts to decrease. This behavior is due to the interaction between the quadrupole moment of SO_2 and the electric dipoles of H_2O molecules, which increases the SO_2 uptake. At higher number of water molecules, water and sulfur dioxide compete for the adsorption sites. For example, at 1 atm, calculations show that increasing the number of H_2O molecules acts to decrease the adsorption of SO_2 in ZTF from ~231 cm^3 (STP) cm^{-3} (without H_2O molecules) to ~150 cm^3 (STP) cm^{-3} (with 100 H_2O molecules). The reduction of SO_2 adsorption at lower pressure in the presence of adsorbed water can be attributed to the stronger binding interactions for H_2O@[Zn^{2+}-Tz] complexes compared to the SO_2@[Zn^{2+}-Tz] ones, whereas at higher pressure the free volume of MOF ZTF contributes to the adsorption capacity as well. Non-bonded interactions between H_2O and ZTF pore are shown in Fig. 12. The H_2O molecules are stabilized in the pores of ZTF with SO_2 molecules by hydrogen bonds between the oxygen of H_2O and the hydrogen of C-(Tz). In the case of H_2S, the presence of H_2O decreases the amount of adsorbed H_2S at 1 atm, whereas at lower pressure, the presence of water molecules slightly increases the adsorption of H_2S similar to the results presented in Fig. 10. This is due to the increased polarity of H_2S in the presence of water at lower pressure. Non-bonded interactions between H_2O/H_2S and the ZTF pore at 1 atm are presented in Fig. 12. We identified the presence of two types of hydrogen bonds: either between the oxygen of H_2O and the hydrogen of

Table 3 Average adsorption amount of SO_2 and of H_2S (in cm^3 (STP) cm^{-3}) in ZTF at $T = 273$ K with and without the presence of H_2O molecules at 0.1 and 1 atm. N_{H_2O} is the number of preloaded H_2O molecules inside the pore

N_{H_2O}	0	10	20	50	100
SO_2 (1 atm)	231	233	213	190	150
SO_2 (0.1 atm)	221	224	220	205	173
H_2S (1 atm)	208	200	193	173	140
H_2S (0.1 atm)	45	46	47	52	58

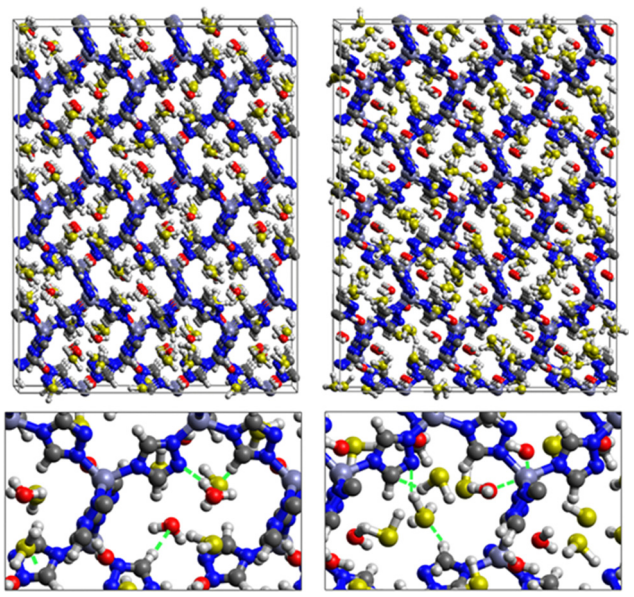

Fig. 11 Top: GCMC adsorption sites of H_2S molecules inside the pores of ZTF in the presence of H_2O near the nitrogen atom of the triazole subunits (left) or near the Zn atom (right). Bottom: Enlargements in the vicinity of H_2S and H_2O where non-bonded interactions are also highlighted.

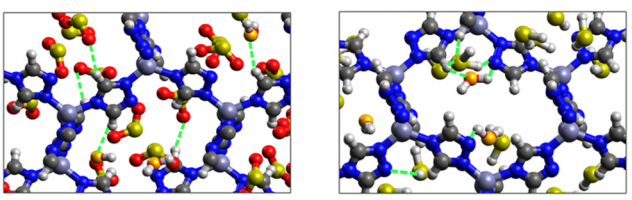

Fig. 12 GCMC adsorption sites of SO_2 (left) and H_2S (right) molecules inside the pores of ZTF in the presence of preloaded H_2O molecules at 1 atm and 273 K. Non-bonded interactions between H_2O and ZTF are also highlighted. Oxygens from H_2O are given in orange.

Table 4 Average adsorption amounts of SO_2 and H_2S (in cm^3 (STP) cm^{-3}) in ZTF at T = 273 K with and without the presence of CO_2 molecules at 1 atm. N_{CO_2} is the number of preloaded CO_2 molecules inside the pore

N_{CO_2}	0	10	20	50	100
SO_2	231	233	213	190	150
H_2S	208	200	192	169	130

C-(Tz) or between the nitrogen of the MOF subunit and the hydrogen of H_2O.

SO_2/H_2S adsorption with a fixed number of preloaded CO_2 molecules inside the ZTF pore. We performed several simulations where we varied the number of the preloaded CO_2 molecules (N_{CO_2}) inside the ZTF cavity. Table 4 gives the results of the SO_2 and H_2S adsorptions in the ZTF model MOF by varying the number of CO_2 molecules from 0 to 100. All simulations were performed at T = 273 K and P = 1 atm. Table 4 shows that increasing the number of CO_2 molecules to up to 10 slightly increases the amount of adsorbed SO_2 (from $\sim$231 to $\sim$233 cm^3 (STP) cm^{-3}). Polarity of SO_2 compared to that of CO_2 plays a key role at low pressure and enhances the adsorption uptake of these molecules in ZTF. Beyond this preloaded amount of CO_2, the SO_2 uptake starts to decrease since at higher number of preloaded CO_2, carbon dioxide and sulfur dioxide compete for the adsorption sites. We can explain this behavior by the stronger interaction between SO_2 and pore surface atoms than in the case of CO_2, which is due to the presence of one strong interaction between one oxygen of SO_2 and zinc of the ZTF pore as discussed above. This behavior was also observed by Ding and Yazaydin.[29] In the case of hydrogen sulfide, the presence of CO_2 in the pore, irrespective of the number of CO_2 molecules, decreases the H_2S adsorption. Indeed, calculations show that increasing the number of CO_2 molecules acts to decrease the adsorption of H_2S in ZTF from $\sim$208 cm^3 (STP) cm^{-3} (without CO_2 molecules) to $\sim$130 cm^3 (STP) cm^{-3} (with 100 CO_2 molecules). The reduction of H_2S adsorption at higher pressures in the presence of adsorbed CO_2 can be attributed to the strong nonbonding interactions[40] of the CO_2@[Zn^{2+}-triazole] ZTF subunit through several types of interactions like electron acceptor–electron donor interactions between the carbon of CO_2 and the nitrogen of Tz of ZTF, π stacking interactions between CO_2 and aromatic rings of Tz and hydrogen bonds. Whereas H_2S is unable to adsorb into the same adsorption positions of the cell as CO_2.

IV. Conclusions

In this work, we used first principles density functional theory calculations and grand canonical Monte Carlo simulations to explore the adsorption properties of SO_2 and H_2S gases with and without the presence of water and carbon dioxide in MAF-66 and ZTF zinc triazolate based frameworks. We have shown here, by using GCMC simulations, that the recently designed ZTF MOF composed of triazolate as the organic ligand and Zn(II) as the metal linker, as well as MAF-66 have good SO_2 and H_2S adsorption capacities at high pressure under dry conditions, at 273 K and 298 K. This sequestration is associated with several types of interactions like hydrogen bonds or electron acceptor–electron donor interactions with the uncoordinated metal sites within these MOFs. Also, we observed that one oxygen of the SO_2 molecule (which acts as the Lewis base) electrostatically interacts with zinc, and therefore SO_2 is physiosorbed rather than chemisorbed avoiding irreversible structural modifications of MOFs and possible drawbacks for recycling these nanomaterials and their subsequent industrial uses. Molecular simulations reveal that the amount of adsorbed gases is closely correlated with the free volume and the accessible surface area, suggesting that the free volume/surface area are important parameters in evaluating SO_2/H_2S gas adsorption capacities.

In general, we established that sulfur dioxide/hydrogen sulphide/carbon dioxide/water compete for adsorption sites. For instance, GCMC simulations of the influence of water on SO_2 adsorption in ZTF, show that water has an unfavorable effect on the capture of SO_2 due to the competition among water molecules to occupy the nitrogens of the triazole ring. In the case of H_2S, the presence of water, however, enhances the adsorption of H_2S for both positions of water inside pores, in agreement with experimental observations. This behavior is confirmed by pre-adsorbing higher amounts of H_2O molecules at a low pressure. At higher pressure and under hydrated conditions, the CO_2 uptake slightly decreases while increasing the number of H_2O molecules. Moreover, our work shows that pre-adsorbing small amount of CO_2 molecules at low pressure increases the capacity of the ZTF for SO_2 uptake, because of the favorable electrostatic interactions between zinc and one oxygen of SO_2. At higher pressure and in the presence of CO_2, the SO_2 uptake slightly decreases while increasing the number of CO_2 molecules. However, the adsorption of H_2S in ZTF in the presence of carbon dioxide is reduced even with a small amount of pre-adsorbed CO_2 molecules.

Conflicts of interest

There are no conflicts to declare.

Acknowledgements

S. G., I. D. J. and M. S. acknowledge support from the Serbian Ministry of Education and Science (Grant no. 451-03-68/2022-14/200026). Numerical simulations were run on the PARADOX-IV supercomputing facility at the Scientific Computing Laboratory, National Center of Excellence for the Study of Complex Systems, Institute of Physics Belgrade, supported in part by the Ministry of Education, Science, and Technological Development of the Republic of Serbia. We thank the COST Action CA21101 – Confined Molecular Systems: from a new generation of materials to the stars (COSY) of the European Community for support.

References

1 P. J. Baxter, J.-C. Baubron and R. Coutinho, *J. Volcanol. Geotherm. Res.*, 1999, **92**, 95–106.
2 M. S. Shah, M. Tsapatsis and J. I. Siepmann, *Chem. Rev.*, 2017, **117**, 9755–9803.
3 M. O. Andreae, *Mar. Chem.*, 1990, **30**, 1–29.
4 T. F. Berglen, T. K. Berntsen, I. S. A. Isaksen and J. K. Sundet, *J. Geophys. Res.*, 2004, **109**, D19310.
5 F. C. Menz and H. M. Seip, *Environ. Sci. Policy*, 2004, **7**, 253–265.
6 B. Liao, Z. Guo, A. Probst and J.-L. Probst, *Geoderma*, 2005, **127**, 91–103.
7 E. Martínez-Ahumada, A. López-Olvera, V. Jancik, J. E. Sánchez-Bautista, E. González-Zamora, V. Martis, D. R. Williams and I. A. Ibarra, *Organometallics*, 2020, **39**(7), 883–915.
8 H. Hikita, S. Asai and T. Tsuji, *AIChE J.*, 1977, **23**, 538–544.
9 R. N. Maddox, G. J. Mains and M. A. Rahman, *Ind. Eng. Chem. Res.*, 1987, **26**, 27–31.
10 Y. S. Mok and H.-J. Lee, *Fuel Process. Technol.*, 2006, **87**, 591–597.
11 S. G. Khokarale and J.-P. Mikkola, *RSC Adv.*, 2018, **8**, 18531–18541.
12 K. Huang, X. Feng, X.-M. Zhang, Y.-T. Wu and X.-B. Hu, *Green Chem.*, 2016, **18**, 1859–1863.
13 Q. Zhang, Y. Hou, S. Ren, K. Zhang and W. Wu, *ACS Sustainable Chem. Eng.*, 2019, **7**, 10931–10936.
14 M. D. Dolan, A. Y. Ilyushechkin, K. G. McLennan and S. D. Sharma, *Asia-Pac. J. Chem. Eng.*, 2012, **7**, 1–13.
15 M. Khabazipour and M. Anbia, *Ind. Eng. Chem. Res.*, 2019, **58**, 22133–22164.
16 P. Cosoli, M. Ferrone, S. Pricl and M. Fermeglia, *Chem. Eng. J.*, 2008, **145**, 86–92.
17 L. Hamon, C. Serre, T. Devic, T. Loiseau, F. Millange, G. Férey and G. D. Weireld, *J. Am. Chem. Soc.*, 2009, **131**, 8775–8777.
18 K. Sumida, D. L. Rogow, J. A. Mason, T. M. McDonald, E. D. Bloch, Z. R. Herm, T.-H. Bae and J. R. Long, *Chem. Rev.*, 2012, **112**, 724–781.
19 T. Baird, K. C. Campbell, P. J. Holliman, R. W. Hoyle, M. Huxam, D. Stirling, B. P. Williams and M. Morris, *J. Mater. Chem.*, 1999, **9**, 599–605.
20 P. R. Westmoreland and D. P. Harrison, *Environ. Sci. Technol.*, 1976, **10**, 659–661.
21 M. Xue, R. Chitrakar, K. Sakane and K. Ooi, *Green Chem.*, 2003, **5**, 529–534.
22 N. E. R. Zimmermann and M. Haranczyk, *Cryst. Growth Des.*, 2016, **16**, 3043–3048.
23 S. Tian, H. Mo, R. Zhang, P. Ning and T. Zhou, *Adsorption*, 2009, **15**, 477–488.
24 J. Guo and A. C. Lua, *J. Colloid Interface Sci.*, 2002, **251**, 242–247.
25 A. Wang, R. Fan, X. Pi, Y. Zhou, G. Chen, W. Chen and Y. Yang, *ACS Appl. Mater. Interfaces*, 2018, **10**, 37407–37416.
26 J. Zhao, A. Buldum, J. Han and J. P. Lu, *Nanotechnology*, 2002, **13**, 195–200.
27 N. S. Bobbitt, M. L. Mendonca, A. J. Howarth, T. Islamoglu, J. T. Hupp, O. K. Farha and R. Q. Snurr, *Chem. Soc. Rev.*, 2017, **46**, 3357–3385.
28 N. C. Burtch and K. S. Walton, *Acc. Chem. Res.*, 2015, **48**, 2850–2857.
29 L. Ding and A. O. Yazaydin, *Phys. Chem. Chem. Phys.*, 2013, **15**, 11856–11861.
30 E. Chen, L. Jia, X. Jia, Q. Wei and L. Zhang, *Chem. Phys. Lett.*, 2021, **778**, 138788–138794.
31 X. Xu, P. Wu, C. Li, K. Zhao, C. Wang, R. Deng and J. Zhang, *Energy Fuels*, 2021, **35**, 5110–5121.
32 C. Wang, H. Xu, P. Huang, X. Xu, H. Wang, Y. Zhang and R. Deng, *Atmosphere*, 2022, **13**, 462–475.
33 X. Zhou, Y. Yu, H. Chen, L. Yang, Y. Qin, T. Wang, W. Sun and C. Wang, *Langmuir*, 2020, **36**, 2775–2785.
34 A. Beheshti, M. Bahrani-Pour, T. Sedaghat, B. Salahshournia, H. Arefi-Nasab, P. Mayer, R. Centore and E. Parisi, *Cryst. Growth Des.*, 2022, **22**, 4343–4356.
35 A. G. Georgiadis, N. Charisiou, I. V. Yentekakis and M. A. Goula, *Materials*, 2020, **13**, 3640.
36 A. Pudi, M. Rezaei, V. Signorini, M. P. Andersson, M. G. Baschetti and S. S. Mansouri, *Sep. Purif. Technol.*, 2022, **298**, 121448-1–1211448-51.
37 X.-D. Song, S. Wang, C. Hao and J.-S. Qiu, *Inorg. Chem. Commun.*, 2014, **46**, 277–281.
38 K. Vellingiri, A. Deep and K.-H. Kim, *ACS Appl. Mater. Interfaces*, 2016, **8**, 29835–29857.
39 S. Bhattacharyya, S. H. Pang, M. R. Dutzer, R. P. Lively, K. S. Walton, D. S. Sholl and S. Nair, *J. Phys. Chem. C*, 2016, **120**, 27221–27229.
40 R. Dahmani, S. Grubišić, I. Djordjević, S. Ben Yaghlane, S. Boughdiri, G. Chambaud and M. Hochlaf, *J. Chem. Phys.*, 2021, **154**(2), 024303.
41 R. Dahmani, S. Grubišić, S. Ben Yaghlane, S. Boughdiri and M. Hochlaf, *J. Phys. Chem. A*, 2019, **123**, 5555–5565.
42 R. Dahmani, S. Ben Yaghlane, S. Boughdiri, M. Mogren Al-Mogren, M. Prakash and M. Hochlaf, *Spectrochim. Acta, Part A*, 2018, **193**, 375–384.
43 J. M. Soler, E. Artacho, J. D. Gale, A. García, J. Junquera, P. Ordejón and D. Sánchez-Portal, *J. Phys.: Condens. Matter*, 2002, **14**, 2745–2779.
44 A. Garcia, *et al.*, *J. Chem. Phys.*, 2020, **152**, 204108-1–204108-31.
45 J. P. Perdew, K. Burke and M. Ernzerhof, *Phys. Rev. Lett.*, 1996, **77**, 3865–3868.
46 W. E. Pickett, *Comput. Phys. Rep.*, 1989, **9**, 115–197.
47 S. L. Mayo, B. D. Olafson and W. A. Goddard, *J. Phys. Chem.*, 1990, **94**, 8897.
48 A. K. Rappe, C. J. Casewit, K. S. Colwell, W. A. Goddard and W. M. Skiff, *J. Am. Chem. Soc.*, 1992, **114**(25), 10024–10035.
49 J. J. Potoff and J. I. Siepmann, *AlChE J.*, 2001, **47**, 1676–1682.
50 F. Sokolic, Y. Guissani and B. Guillot, *Mol. Phys.*, 1985, **56**, 239–253.
51 M. C. C. Ribeiro, *J. Phys. Chem. B*, 2006, **110**, 8789–8797.

52 K. N. Shyamal, *J. Phys. Chem. B*, 2003, **107**, 9498–9504.
53 X. Peng and D. Cao, *AIChE J.*, 2013, **59**, 2928–2942.
54 W. L. Jorgensen, J. Chandrasekhar, J. D. Madura, R. W. Impey and M. L. Klein, *J. Chem. Phys.*, 1983, **79**, 926–935.
55 D. Dubbeldam, A. Torres-Knoop and K. S. Walton, *Mol. Simulat.*, 2013, **39**, 1253–1292.
56 D. Dubbeldam, S. Calero, D. E. Ellis and R. Q. Snurr, *Mol. Simulat.*, 2016, **42**, 81–101.
57 R. B. Lin, D. Chen, Y. Y. Lin, J. P. Zhang and X. M. Chen, *Inorg. Chem.*, 2012, **51**, 9950–9955.
58 H. Y. Zhang, Z. R. Zhang, C. Yang, L. X. Ling, B. J. Wang and H. L. Fan, *J. Inorg. Organomet. Polym. Mater.*, 2018, **28**, 694–701.